Snow characterization at a global scale with passive microwave satellite observations

E. Cordisco,[1] C. Prigent,[1] and F. Aires[2]

[1]   The sensitivity of passive microwave satellite observations to snow characteristics is evaluated, between 19 and 85 GHz, for a winter season, for the Northern Hemisphere. The surface emissivities derived from the Special Sensor Microwave/Imager measurements are systematically compared with in situ snow measurements at 2784 stations, in North America and Eurasia. In addition, coincident satellite responses from active microwave sensors (ERS scatterometer) and visible observations (AVHRR) are also analyzed. Vegetation interferes with the signal that is received by the satellites. Snow emissivities also react to scattering by the snow grain growth that is related to the snow metamorphism during the winter. This phenomenon increases with frequency and is already very sensitive at 37 GHz. Passive microwaves at high frequency (85 GHz) are very sensitive to the presence of snow on the ground, even for very low snow depth. None of the tested satellite measurements is well correlated to the snow depth at a global scale, making snow depth retrieval from these observations very difficult on a global basis. The sensitivity of the satellite observations to snow characteristics depends on local conditions. To partly alleviate these difficulties, a neural network inversion scheme based on local statistics is developed to combine satellite observations, in situ measurements, and land surface model outputs. The combination of different wavelengths partly limits the ambiguities related to the individual sensitivity of each satellite observation to the various sources of variabilities. The final retrieval algorithm is compatible with an assimilation strategy that would better constrain the behavior of surface models. Finally, a clustering algorithm is applied to the suite of satellite observations and clearly shows a strong sensitivity to the snow characteristics and metamorphism during the winter. Characterization of the snowpack using satellite observation classification can yield qualitative information for snow model parameterization.

1.   Introduction

[2]   The land area covered by snow in the Northern Hemisphere ranges from $\sim 4.10^6$ km^2 at its minimum in August to $\sim 47.10^6$ km^2 at its maximum in January [*Robinson et al.*, 1993]. Because of its high albedo, snow extent is a primary factor controlling the amount of solar radiation absorbed by the Earth. Even a shallow snow cover can increase the albedo of a bare landscape from 0.2 to 0.8. Any decrease in snow cover related to a warming trend results in increased absorption of solar radiation, melting the snow and inducing a positive feedback. As a conse-quence, the cryospheric components of the climate are regarded as sensitive indicators of changes. Snow cover also interacts with and modifies the overlying air masses, considerably influencing the atmospheric circulation, not only in polar regions but also at midlatitudes, making assimilation of observations in polar regions crucial for Numerical Weather Prediction (NWP) models. The snow cover as well as the snow depth, its albedo and other thermal characteristics are of importance in the interaction with the atmosphere [*Gong et al.*, 2004]. In addition, snow is a dominant source of delayed water supply in the northern regions, with large impact on the global hydrological budget. *Sud and Mocko* [1999] insist on the influence of the snow melting processes on modeled soil moisture.

[3]   A snowpack is a complex medium with large spatial and temporal variability [*Frei and Robinson*, 1999]. It can consist of several layers having different densities and crystal-size distributions. The properties of these layers reflect the snowpack history and relate to location and elevation. *Sturm et al.* [1995], for instance, suggest sepa-

[1]Centre National de la Recherche Scientifique, Laboratoire d'Etudes du Rayonnement et de la Matière en Astrophysique, Observatoire de Paris, Paris, France.
[2]Centre National de la Recherche Scientifique/Institut Pierre-Simon Laplace/Laboratoire de Météorologie Dynamique, Université Paris VI, Paris, France.

rating the snow into six classes (tundra, taiga, alpine, maritime, prairie, and ephemeral), each type having a unique ensemble of textural and stratigraphic characteristics, including the sequence of snow layers, their thickness, density, crystal morphology, and grain size.

[4] Unfortunately, conventional measurements in remote polar areas are sparse, thus limiting the ability to accurately monitor the snow characteristics, its coverage, its depth, and season length. In addition, point measurements are often considered not suitable for regional and continental applications. Satellite observations provide a unique opportunity to continuously monitor the whole polar region at regional scales.

[5] Microwave radiation responds to snow properties such as density, depth, crystal-size distribution, vertical temperature gradient, surface wetness, melting-refreezing cycles, and embedded or covering vegetation. The responses of microwave radiation to these surface characteristics are usually highly dependent on frequency. An extensive amount of research has been directed toward a better understanding of the mechanisms responsible for the microwave emission of snow, from both modeling analysis and ground based or aircraft experiments. Modeled microwave emissivities of snow are particularly sensitive to snow water equivalent, grain size, and snow wetness. The dielectric losses in dry snow are very small, so the extinction coefficient is dominated by scattering, this effect being stronger at shorter wavelengths, for larger particles and drier snow. The first numerical results for dry snow used conventional Mie scattering theory and predicted a steep decrease of the brightness temperatures with grain size [e.g., *Chang et al.*, 1976]. Calculations using dense-medium theory show that the scattering is less than predicted with the assumption of independent scattering assumed by the Mie scattering theory [e.g., *Tsang*, 1992]. Large differences in the dielectric properties of liquid and frozen water at microwave frequencies produce substantial variations of the snow emissivity with wetness and melting. With increasing wetness, the dielectric losses become large and the scattering negligible. Wet snowpacks radiate like black bodies at the physical temperature of the upper snow layer. In the spring, snow undergoes melting and refreezing cycles during which large spherical grains are formed. Grain sizes can increase by a factor of 2–3 by the end of the winter [*Sturm and Benson*, 1997]. Thus the microwave signature of the snowpack varies between black body behavior for wet snow to high reflectivities due to strong volume scattering by the large heterogeneities. This effect is especially sensitive at higher frequencies. Field experiments have been conducted to analyze the snow emissivity with respect to the characteristics of the snowpack. The University of Bern has been particularly active with ground-based measurements in the Alps [e.g., *Schanda et al.*, 1983; *Matzler*, 1994]. The University of Helsinki and the UK Met Office conducted several aircraft measurement campaigns [e.g., *Kurvonen and Hallikainen*, 1997; *Hewison and English*, 1999]. Measurements confirm the large variability of the snow emissivities with snow characteristics and history. *Matzler* [1994] measured emissivities of various landscapes in winter between 5 and 100 GHz at 50° incidence and searched for specific microwave signatures that would enable unambiguous retrieval of snow parameters from

microwave observations. He concluded that estimation of snow water equivalent is not feasible solely from passive microwave observations in this range. However, snow cover can be discriminated from other surfaces, even for fresh powder snow when using the higher frequencies. Passive microwave satellite observations over snow have been used to estimate snow cover and depth [e.g., *Kunzi et al.*, 1982; *Chang et al.*, 1987; *Hall et al.*, 1991; *Foster et al.* 1996a; *Grody and Basist*, 1996; *Pulliainen and Hallikainen*, 2001; *Josberger and Mognard*, 2002], with the substantial advantages over visible observations that the microwave observations do not depend on the solar illumination, are not limited to cloud-free areas, and are sensitive to snow depth. However, global applications of snow depth algorithms are questioned and several studies have suggested the need for regionally specific adjustments [*Foster et al.*, 1996b; *Robinson and Spies*, 1994] or for adding extra information in the retrieval process (e.g., land classification, topography, air temperature [*Singh and Gan*, 2000] or temperature history [*Josberger and Mognard*, 2002]). In addition, compared to visible or infrared observations, microwave observations have coarser spatial resolution, creating problems when interpreting heterogeneous footprints that cover mixtures of surface types and snow characteristics.

[6] The objective of this study is to investigate the sensitivity of passive microwave satellite observations between 19 and 85 GHz to snow properties on a global basis for a whole winter (1992–1993) with the help of ancillary information to better characterize the parameters that influence the microwave responses over snow. Passive microwave information is provided by the SSM/I from which the microwave land surface emissivities are calculated [*Prigent et al.*, 1997, 2001]. The in situ snow measurements, the satellite observations and the ancillary data sets are described in section 2. Section 3 presents the observations analysis, with special emphasis on the spatial and temporal variability of the emissivity over snow-covered regions. Section 4 examines the possibility to retrieve snow depth and water equivalent from satellite observations. In addition, a snow classification based on microwave emissivity is proposed in section 5 and is compared to the classification of *Sturm et al.* [1995]. Section 6 concludes this study.

2. Passive Microwave Satellite Observations, In Situ Measurements, and Ancillary Data Sets

[7] This study examines passive microwave satellite data in coincidence with a large data set of in situ snow measurements. Ancillary information concerning vegetation and topography helps analyze the microwave signal. The *Sturm et al.* [1995] classification gives insight into the snow microphysical properties. For comparison purposes, coincident ERS scatterometer observations and visible reflectances is also analyzed.

2.1. Passive Microwaves: SSM/I Emissivities Between 19 and 85 GHz

[8] The SSM/I instruments on board the Defense Meteorological Satellite Program (DMSP) polar orbiters observe the Earth twice daily at 19.35, 22.235, 37.0, and 85.5 GHz with both vertical and horizontal polarizations, with the exception of 22 GHz which is vertical polarization only.
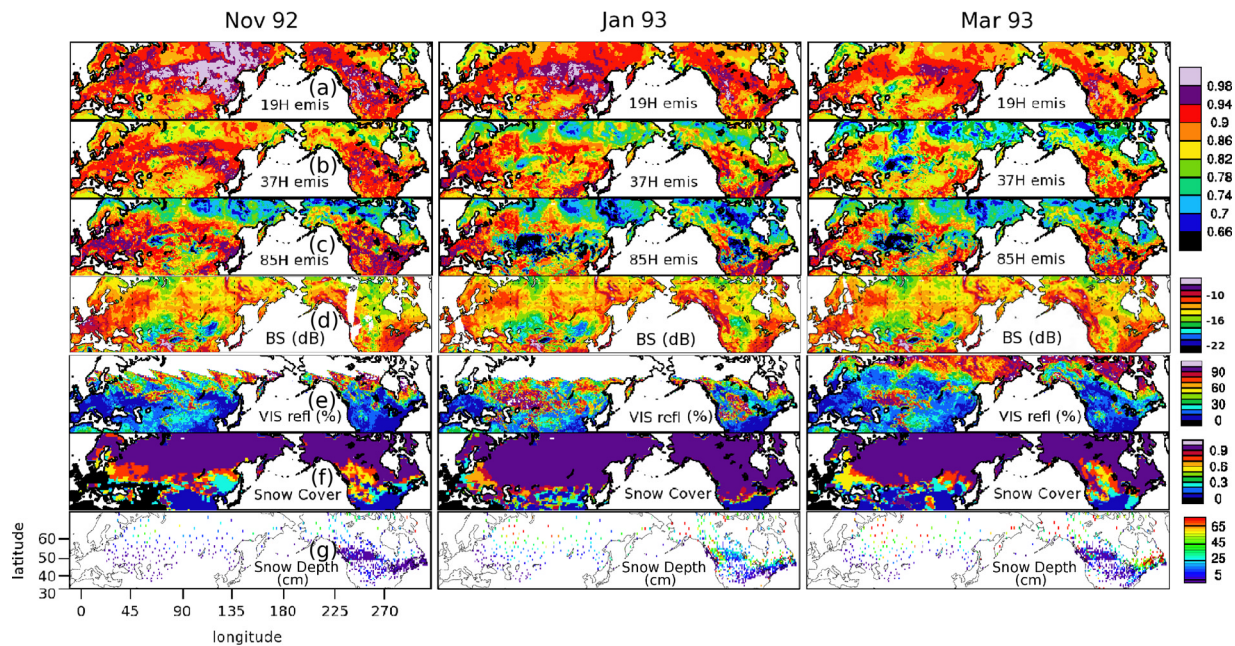
Figure 1. Monthly mean effective emissivities at (a) 19, (b) 37, and (c) 85 GHz for horizontal polarization from SSM/I; (d) the ERS scatterometer backscattering coefficient interpolated at 45° incidence angle in dB; (e) the visible reflectances from AVHRR in percentage; (f) NOAA snow cover product; and (g) the in situ snow depth at the local stations in centimeters. The results are presented for November 1992, January 1993, and March 1993, from left to right.

The observing incidence angle is close to 53°, and the fields of view decrease with frequency, from 43 km × 69 km to 13 km × 15 km [*Hollinger et al.*, 1987]. Brightness temperatures are often directly used in snow characterization algorithms. They include the contribution from the atmosphere and potentially from clouds. *Prigent et al.* [1997, 2001] estimate microwave emissivities of land surfaces from SSM/I observations by removing contributions from the atmosphere, clouds, and rain using ancillary data from the International Satellite Cloud Climatology Project (ISCCP) [*Rossow and Schiffer*, 1999] and the NCEP reanalysis [*Kalnay et al.*, 1996]. Cloud-free SSM/I observations are first isolated using collocated visible/infrared satellite observations (ISCCP data). The cloud-free atmospheric contribution is then calculated from an estimate of the local atmospheric profile from NCEP reanalysis. Finally, with the surface skin temperature derived from IR observations (ISCCP estimate), the surface emissivity is calculated for the seven SSM/I channels. The calculated emissivities are related to the surface properties themselves, decontaminated from atmospheric contributions or from modulations by the surface temperature T_s. They are estimated on an equal area grid of 0.25° × 0.25° at the equator, each pixel covering 773 km². Monthly mean emissivities (at 53° incidence angle) are presented in Figure 1 at 19 GHz (Figure 1a), 37 GHz (Figure 1b), and 85 GHz (Figure 1c) for the horizontal polarization, for November 1992, January 1993, and March 1993.

2.2. In Situ Snow Measurements

[9] We consider three sources of in situ data: the Canadian Daily Snow Depth Database established for the CRYSYS project from Environment Canada [*Brown*, 2000], the snow depth station measurements gathered by the National Centers for Environmental Prediction over North America, and the Historical Soviet Daily Snow Depth [*Armstrong*, 2001]. The in situ snow depth measurements cover Canada (2032 stations), USA (552 stations), and the former Soviet Union (200 stations) during the 1992–1993 snow season, with an accuracy of 2.54 cm (1 inch) in the USA and 1 cm elsewhere. We carefully quality-control the measurements and all anomalous measurements are rejected. American and nearly 250 Canadian stations include the air temperature at 2 m above ground level.

[10] Comparisons between satellite and point measurements are challenging because of the differences in spatial scales [*Brubaker et al.*, 2000]. In this study, no spatial interpolation has been applied and only coincident measurements are analyzed. For monthly mean snow depth calculations, we only consider the stations with at least 10 measurements during the month. For comparison with the satellite observations, for each box of the equal area grid of 0.25° × 0.25° at the equator, the in situ measurements are averaged. Figure 1g shows the monthly mean snow depth for November 1992, January 1993, and March 1993. The in situ measurements cover a large variety of environments in the Northern Hemisphere, for a whole winter season.

[11] Snow water equivalent is also measured at 672 stations in Canada, every 2 weeks with an accuracy of 1 mm [*Schmidlin*, 1990]. These measurements provided by the Canadian Meteorological Service result from the melting of five snow cores near the station. The density of new snow ranges from about 50 kg.m^{-3} when the air temperature is low, to about 200 kg.m^{-3} when the temperature is close to
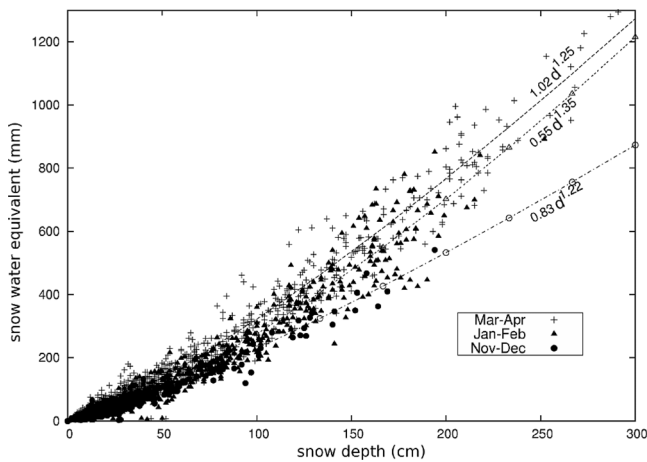
Figure 2. Relationship between snow depth (d) and snow water equivalent as derived from the available measurements in Canada for the winter 1992–1993. The measurements are separated by months and a regression is given for each winter period: beginning (circles), middle (triangles), and end (crosses) of the winter.

0°C. Snow density increases with time after snow fall, because of gravitational settling, wind packing, melting, and recrystallization. The relationship between snow depth and snow water equivalent is presented in Figure 2 for all the available measurements. As the density of the snow changes with depth, the relationship between snow water equivalent and snow depth is not linear, with density increasing with snow depth. In addition, as expected, during the winter season for a given snow depth, the snow water equivalent increases, as shown in Figure 2 from the in situ measurements.

[12] The operational NOAA snow data product is also presented in Figure 1f, as the percentage of time during a month that a given pixel is snow covered. The NOAA Northern Hemisphere Weekly Snow and Ice Cover Charts are prepared from inspection of all available visible satellite imagery on a daily basis.

2.3. Ancillary Information
2.3.1. Vegetation Classification and Topography
[13] *Matthews* [1983] vegetation and land use data sets are compiled from a large number of published sources. At a 1° spatial resolution the vegetation classification distinguishes a large number of vegetation types, that are further grouped into 9 classes [*Prigent et al.*, 2001]. Associated with the vegetation classification is a land use data set that distinguishes five levels of cultivation intensity, ranging from 0 to 100% cultivation for 1° cells. Combining the vegetation and land use data set gives information about the actual land cover. For each vegetation class, areas with cultivation intensity greater than 20% are defined as cultivation, which makes up a tenth class. For topography information, the Global Land One-kilometer Base Elevation (GLOBE) digital elevation model with a 30″ spatial sampling is used.
2.3.2. Sturm et al. [1995] Snow Classification
[14] A snow cover classification is proposed by *Sturm et al.* [1995]. It is a unified compilation of different classi-

fications in which each class is uniquely defined by a set of textural and stratigraphic properties of the snow. Six classes are identified (tundra, taiga, maritime, prairie, mountain, and ephemeral), each one having representative densities, grain size, stratigraphy, and thermal properties. Each class is simply related to climate regime and the snow cover class can be inferred from routinely measured variables such as wind, air temperature, and precipitation. The derived classification is available with a 0.5° spatial resolution.
2.3.3. ERS Backscattering Coefficient
[15] The European Remote Sensing (ERS) polar orbiters provide observations in the active microwave domain at 5.25 GHz. The scatterometer nominal spatial resolution is 50 km and the observations are gridded on the equal area grid of 0.25° × 0.25°. For each grid point, the backscattering coefficients are considered for all incidence angles and a linear angular regression is used to estimate the corresponding monthly mean backscattering coefficient at 45° [*Prigent et al.*, 2001]. Figure 1d shows the resulting backscattering coefficient for 3 months during the winter season.
2.3.4. AVHRR Visible Reflectances
[16] The Advanced Very High Resolution Radiometer on board the NOAA meteorological polar orbiters provides daily observations of the Earth in the visible (0.58–0.68 micron). The monthly composite AVHRR visible reflectances generated under the joint NASA and NOAA Earth Observing System Pathfinder project [*James and Kalluri*, 1994] are used in this study. We average the nominal 8 km Pathfinder resolution to the resolution of the equal area grid. Figure 1e shows the resulting visible reflectances for the 3 months.

3. Analysis of the Spatial and Temporal Variability of the Passive Microwave Signatures Over Snow

[17] First, satellite signatures over snow have a large spatial variability, in the microwave and in the visible, for a given month (Figure 1). In March for instance, the region North of 50°N is almost completely covered by snow during the whole month but shows very contrasted responses at all frequencies. As an example, the plains in Kazakhstan north of the Aral Sea are associated with very high visible reflectances and low emissivities (especially at 85 GHz), whereas low reflectances and higher emissivities are observed in Siberia around 60°N. There is also a sharp discontinuity in the signatures of passive and active microwaves at a given latitude from the east to the west of the Ural mountains. In January in North America, north of 45°N, contrasted signatures are observed even in the visible, although the snow cover is total. Second, for a given region, the satellite observations can undergo significant changes during the winter season, without large variations in the snow cover or snow depth. The Labrador in Canada is such a region, with large temporal variations in the emissivity even at 19 GHz, although the snow cover is constant and the snow depth does not vary much.

[18] What are the variations in the snowpack characteristics that explain these differences in the satellite responses?
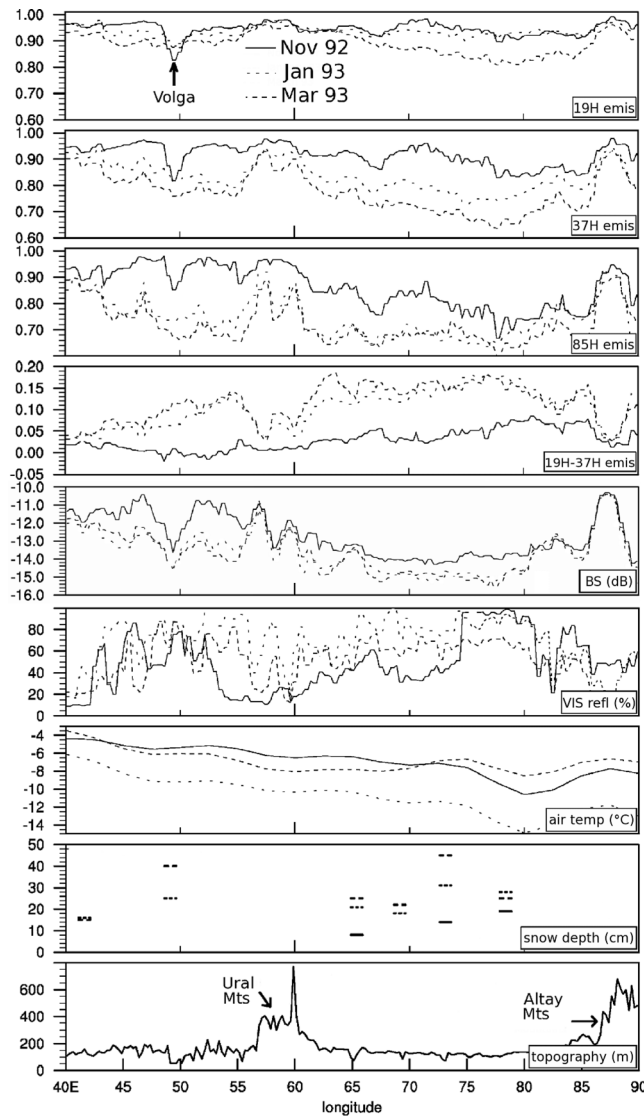
Figure 3. Cross section of the various monthly mean measurements at 55.5°N in Russia between 40 and 90°E. From top to bottom are the SSM/I microwave emissivities at 19, 37, and 85 GHz (horizontal polarization) along with the emissivity difference between 19 and 37 GHz; the ERS scatterometer backscattering coefficient interpolated at 45° incidence angle and the AVHRR visible reflectances; the ECMWF surface air temperatures; the in situ snow depth at the local stations; and the topography. Most variables are presented for November 1992, January 1993, and March 1993.

[19] The monthly mean satellite-derived parameters and ancillary information are compared along a cross section at 55°N in Russia, for the 3 months previously considered (Figure 3). Snow totally covers the region for this whole period. Along with the microwave and visible satellite information (the first six plots), the snow depth at the stations, the air temperature (from the ECMWF reanalysis), and the topography are indicated. Several noticeable geographical features can be mentioned: the Ural Mountains (between 55 and 60°E), the Altay Mounts (between 85 and 90°E), or the Volga River (~49°E). Mountains are characterized by an increase in the backscattering coefficient and in the microwave emissivities, due to the sensitivity of these measurements to the topographic roughness. However, the snow signatures at 37 GHz and 85 GHz are still observable over the Ural (the signal is much weaker over the Altay Mounts likely because of denser vegetation). In November, the emissivities decrease over rivers: the dielectric properties of water induce low emissivities that contrast with the surrounding areas. For the rest of the winter, the rivers are frozen and/or snow covered and they do not have distinct signatures. In rather flat regions, the backscattering and the microwave emissivities decrease with time during the winter season. By the end of the winter, larger snow grains are formed [Sturm and Benson, 1997]: the microwave signature of the snowpack then varies between the characteristic of wet snow in November to lower emissivities due to scattering by the large heterogeneities by the end of the winter. East of the Ural Mountains, the emissivity decrease at the end of the snow season is more pronounced than on the west: even at 19 GHz, significant scattering is observed in March between 65 and 85°E. This is consistent with the snow classification by Sturm et al. [1995] that distinguishes between mostly "prairie" snow west of Ural and mostly "tundra" snow east of the mountain range. By late winter, "tundra" snow contains a large percentage of depth hoars that cause scattering even at 19 GHz. The lower mean air temperatures observed east of the mountain is also consistent with this snow type, the lowest temperature coinciding well with the lowest observed emissivities (i.e., corresponding to the highest probability of depth hoar formation). The differences between 19 and 37 GHz have often been used as representative of the snow depth variations [Chang et al., 1987]: on this cross section, this relationship between the satellite data and the in situ snow depth measurements is not clear. East of the Ural Mountains, vegetation is dominated by deciduous forest whereas cultivation and grassland prevail in the west [Matthews, 1983]. As expected, for similar snow depth, the sensitivity of the emissivities to the snow signal is more pronounced where the vegetation density is lower. The visible reflectances also show large variations along this cross section during the winter. The reflectances increase from November to the middle of the winter, then decrease by the end of the winter although snow still covers the surface. This is expected as the concentration of snow impurity (deposition of dust and vegetation debris) and grain size increase with snow aging and reduces the snow visible reflectances [Aoki et al., 2000].

[20] The effect of vegetation on the snow emissivities is illustrated in Figure 4. In the region between 60–90°E and 52–63°N where the snow cover and topography are rather homogeneous, the normalized histograms of various satellite observations are presented for three types of vegetation in January 1993. Cultivation, grassland, and tundra correspond to low vegetation density, especially in winter. The density of the vegetation cover is high all year long for evergreen forest. The deciduous forest in winter corresponds to an intermediate vegetation density between the two previous ones. The sensitivity of the snow emissivity to vegetation density increases with frequency, with the 19 GHz only weakly responding to the vegetation changes.
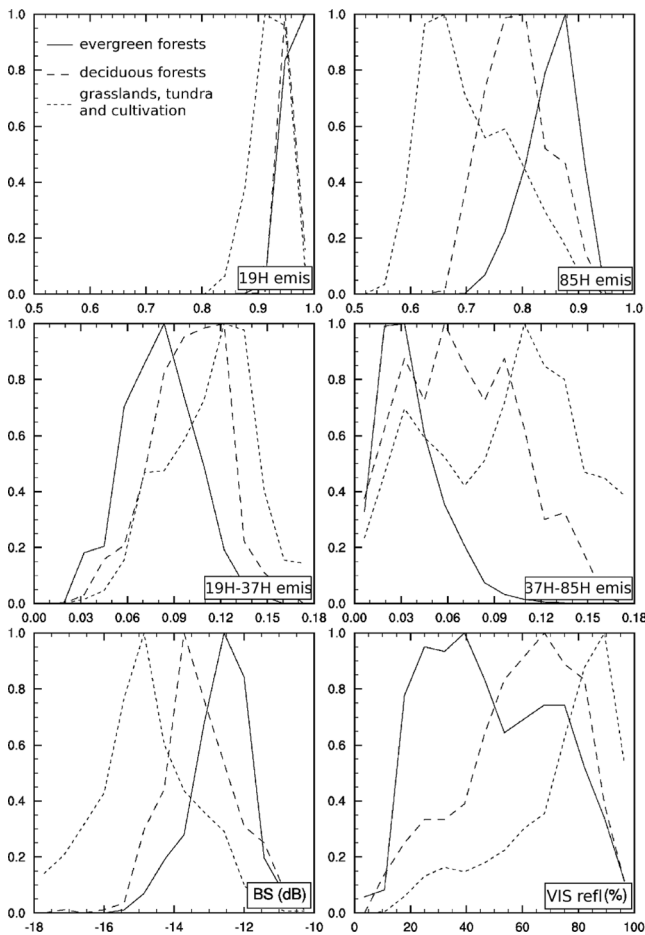
Figure 4. Normalized histograms of the SSM/I microwave emissivities, ERS backscattering coefficients, and the visible reflectances for three types of vegetation, for January 1993 for all the pixels that are fully snow covered in the area between 60 and 90°E and 52 and 63°N.

At 85 GHz, the presence of dense evergreen vegetation increases the emissivity, as expected: emissivity histograms of evergreen forested areas are well separated from the other two that correspond to lower density vegetation cover, during winter time. The 19H−37H and 37H−85H emissivity differences are also very sensitive to the presence of vegetation, confirming that these differences are not simply and uniformly proportional to the snow depth. In active microwave, the backscattering decreases because of the presence of the snow on a low topographic roughness but this decrease is limited by vegetation influence. In the visible as well, the effect of the vegetation cover is evident, with the reflectances decreasing with increasing vegetation density.

[21] To further investigate the mechanisms that drive the relationship between satellite observations and in situ measurements, time series for each variable are presented at two selected sites (Figure 5 (left) in Siberia 134.75°E 60.37°N and Figure 5 (right) in Canada 80.70°W 51.39°N). The microwave emissivities are calculated for all clear sky situations. Monthly mean visible reflectances are added to the figures for comparisons. Compared to the lowest fre-

quencies, the 85 GHz reacts much more strongly to the first centimeters of snow on the ground, with sharply decreasing emissivities as soon as snow appears. It then reaches a minimum (around beginning of December in Siberia) and stabilizes although the snow depth keeps increasing. This behavior has also been observed by *Rosenfeld and Grody* [2000]. The 37 and 19 GHz emissivities also decrease during the winter season but with a much lower rate. For
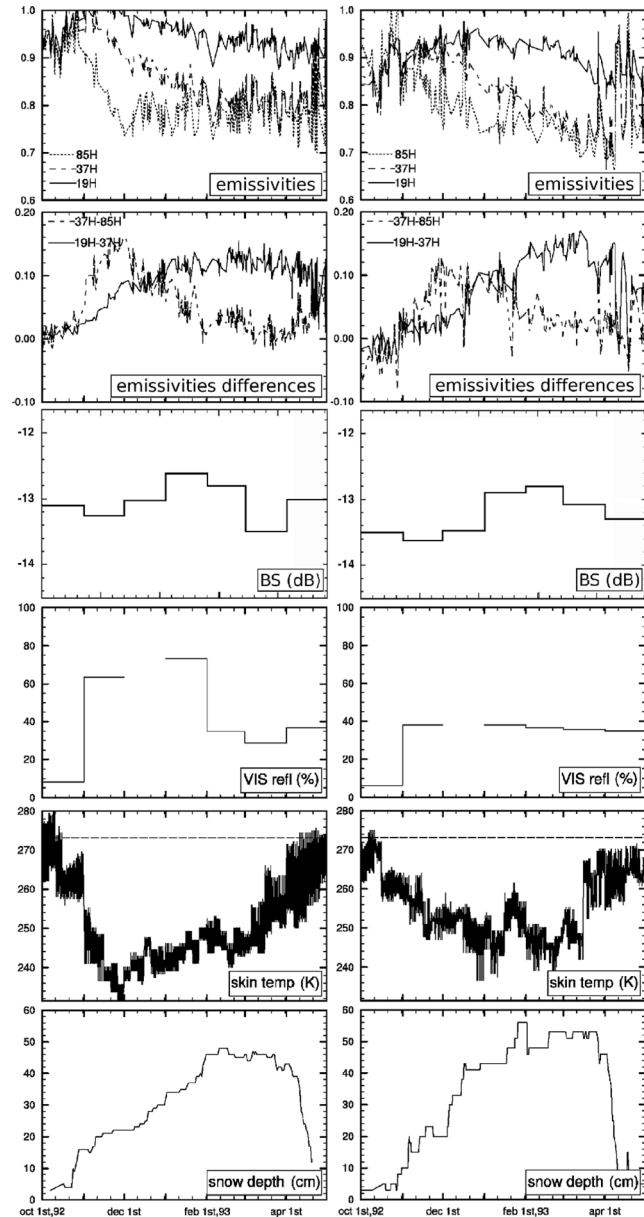
Figure 5. Time series of the various measurements from October 1992 to May 1993 for two locations: at 134.0°E 60.4°N (deciduous forests) in Russia and at 80.7°W 51.4°N (evergreen forests) in Canada. From top to bottom are the microwave emissivity daily estimates (clear sky only) at 19, 37, and 85 GHz for the horizontal polarization; the daily emissivity differences for horizontal polarization; monthly mean ERS backscattering; monthly mean AVHRR visible reflectances; the surface skin temperature from ISCCP; and the in situ snow depth measurements.
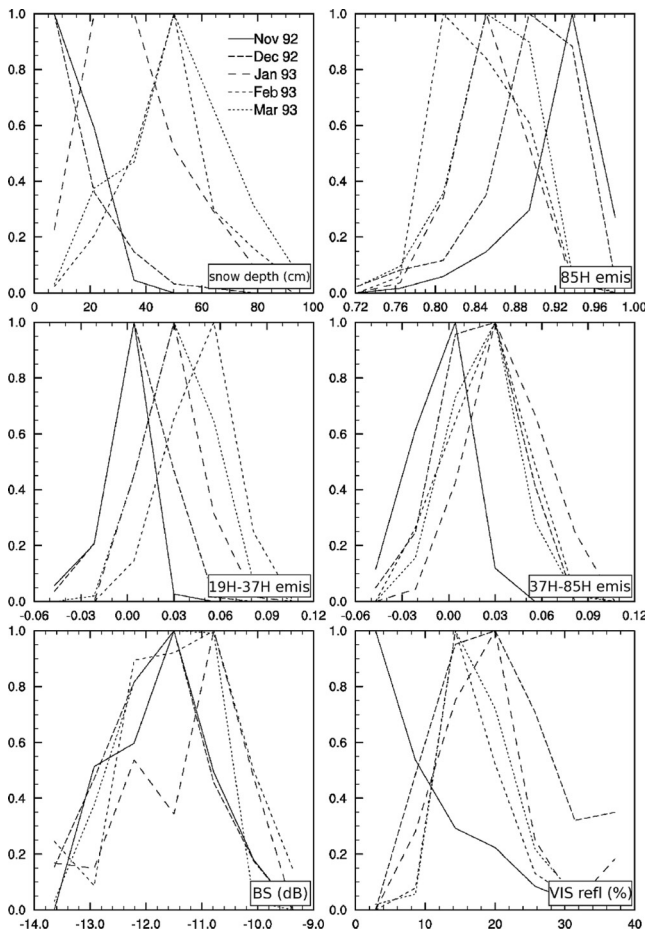
Figure 6. Same as Figure 4 but for 5 months during snow season in North America (92.7°W 88.9°W 49.1°N 52.89°N) over evergreen forest.

these two cases, the 37 and 85 GHz emissivities are similar around February. In Siberia, the emissivity difference at 19 and 37 GHz smoothly increases with snow depth. As the skin temperature approaches melting at the end of the winter, the emissivities strongly vary from a day to the other. The thawing transition induced a rather strong defect on the microwave signal, as already explored by *Judge et al.* [1997] to classify the freeze/thaw prairie soils with SSM/I. The backscattering coefficient and the visible reflectances increase as the snow covers the surface but decrease in February, although snow still covers the area. This phenomenon coincides with the sharp decrease in the emissivity difference between 37 and 85 GHz. The visible reflectances are expected to be sensitive to dust deposition on the surface and to a lesser extent to snow grain variations. Given that the difference between 37 and 85 GHz is likely driven by snow particle metamorphism, the impact of the snow grain on the visible reflectances is suspected to be significant as well.

[22] Figure 6 presents the histograms of the satellite responses for the different winter months over a fully snow covered region (located between 263–297°E and 46–52°N). The emissivities decrease from November to February but start increasing in March, when the snow depth is still increasing. This change in the behavior also appears on

the differences between the 19 and 37 GHz. *Kelly and Chang* [2003] also report on an "hysteresis" phenomenon: the difference between the brightness temperatures at 19 and 37 GHz increases with increasing snow depth during the first part of the winter, but after a maximum, it decreases more rapidly than the measured snow depth. They actually do not apply their regression algorithm to the late winter period because of this phenomenon. *Rosenfeld and Grody* [2000] also insist on this aspect that they characterize as an anomalous signature. Similar phenomenon appears on the visible reflectances.

4. Information Content of Satellite Observations on Snow Depth

[23] Snow Depth (SD) is a key characteristic of the snowpack that plays important roles in land surface and hydrological models. The relationship between this quantity and the satellite observations is now examined.

[24] First, we calculate the linear correlation between the various satellite products and the snow depth, on a monthly mean basis, for the 1992–1993 winter for all the available station measurements. Emissivity combinations are also considered. Most algorithms to retrieve snow depth and water equivalent from passive microwaves are based on a linear function of the brightness temperatures between 19 and 36 GHz, usually for horizontal polarization [*Chang et al.*, 1987]: SD (cm) = $a \cdot (T_b18H - T_b36H) + b$. In the initial algorithm, a is fixed to 1.59 cm.K^{-1} with the assumption that the grain radius is 0.3 mm and the snow density is 300 kg.m^{-3}. Table 1 summarizes the results of the linear regression calculations. Whatever the satellite variable, the linear correlations are very low (maximum of 0.26 for the backscattering coefficients) on a global basis, showing that the snow depth will be difficult to retrieve globally from simple and unique satellite information. Limiting the correlation calculations to a given winter period (beginning, middle, and end of the winter) does not improve the correlation significantly. Restricting the calculation to low vegetation density and to a specific period during the winter increases the linear correlation, but remains too low to warrant a quality retrieval even in sparsely vegetated regions. *Rosenfeld and Grody* [2000] also find very low and changing correlations during the winter between the brightness temperatures and the snow depth.

[25] Considering the questionable applicability of the static method to the globe, *Kelly and Chang* [2003] revisit it by tuning the coefficient a and b in the previous equation for each region and considering a vegetation cover. They observe that errors are slightly smaller with this "dynamic" algorithm than with the "static" one, especially at the begin of the snow season. *Josberger and Mognard* [2002] also develop an algorithm. It is based on the *Chang et al.* [1987] approach but parameterized with the temperature gradient between the air and the ground, to account for the dependence of the microwave scattering on the snow grain size. The method has been evaluated over Siberia [*Grippa et al.*, 2004] and again, it performs sightly better than the static algorithm for the first part of the snow season but not for the second part of the winter, when the snow has already undergone metamorphism. *Kelly et al.* [2003] model the grain radius growth and the snow densification process to

Table 1. Linear Correlation Between the in Situ Snow Depth and, From Top to Bottom, Monthly Mean Effective Emissivities at 19 GHz, 37, and 85 GHz for Horizontal Polarization and for Frequency Differences From SSM/I, ERS Scatterometer Backscattering at 45°, Visible Reflectances From AVHRR[a]

Snow Depth Versus	Global	Winter Period			Vegetation Density	
		Oct to Dec	Jan	Feb to May	High	Low
Emissivity at 19H	−0.06	−0.03	0.11	−0.01	0.12	−0.05
Emissivity at 37H	−0.12	−0.21	−0.01	0.08	−0.01	−0.23
Emissivity at 85H	0.04	−0.14	0.13	0.18	0.04	0.21
Emissivity at 19H−37H	0.11	0.31	0.15	−0.13	0.21	0.29
Emissivity at 37H−85H	−0.21	0.02	−0.20	−0.26	−0.07	−0.49
Backscattering	0.26	0.15	0.27	0.30	0.22	0.19
VIS reflectance	−0.04	0.16	−0.05	−0.04	0.14	−0.13

[a]Results are presented globally and then for different winter periods and vegetation densities.

parameterize their initial static model, but the new model does not show significant improvement over the static algorithm. They insist on the fact that locally the algorithms can perform better.

[26] For each selected in situ station, we calculate the linear correlations between the 19 and 37 GHz emissivity difference and the snow depth during the winter. Locally, good correlations are obtained (Figure 7). From one location to another, the satellite observations are affected by different sources of variability, the snow depth being one among several others like the vegetation. At a given location, there is a reduced number of sources of variability and the correlation between the in situ snow depth measurements and the satellite observations is much larger. The global correlations are recalculated, subtracting for each location and each observations the mean value over the winter and normalizing them by the standard deviation for that location (Figure 8). The linear correlation is larger (0.6). This local standardization procedure has the effect of partly suppressing the variability that is location-dependent (see *Aires et al.* [2005] for the same approach in a soil moisture study).

[27] This means that locally snow depth information could realistically be extracted from the passive microwave observations, provided that statistics on the snow depth in the region are available (mean and standard deviation of the snow depth during the winter). This information is obviously available at the in situ measurement stations. Is it possible to interpolate this information in space? *Cline and Carroll* [1999] or *Brubaker et al.* [2000] use pure statistical spatial interpolation method based on kriging. For instance, *Cline and Carroll* [1999] obtain gridded snow water equiv-

alent estimates in the upper Mississippi River Basin from ground-based and remotely sensed snow data. If information on the spatial patterns of the snow depths can be obtained, then the local statistics could be interpolated in space which would allow to apply the retrieval process outside the in situ stations. To examine this possibility, we analyze the outputs from a land surface model. ISBA-ES (Interactions between Soil, Biosphere and Atmosphere–Explicit Snow) [*Douville et al.*, 1995; *Boone and Etchevers*, 2001] includes a so-called intermediate complexity snow scheme, to better understand which snow processes are the most important for atmospheric and macroscale hydrological applications. An explicit multilayered approach resolves the large vertical density and temperature gradients, distinguishes the thermal properties between the snow and the soil-vegetation layer, includes the effects of liquid water transmission and storage refreezing in the snow pack, and models the absorption of incident radiation within the snowpack. We study ten years of ISBA-ES snow depth outputs, on a monthly mean basis with a $1° \times 1°$ spatial resolution. A Principal Component Analysis (PCA) is performed on this database to identify the predominant spatial patterns, globally, and separately on the Eurasia and North America.

[28] For the three situations, the first component explains ~75% of the variance and clearly indicates a latitude gradient whereas the second component (representing less than 10% of the variance) shows more complex structures partly related to the topography and distance to the coasts. Higher order components are less interpretable but for a good representation of the spatial variability of ISBA, 50
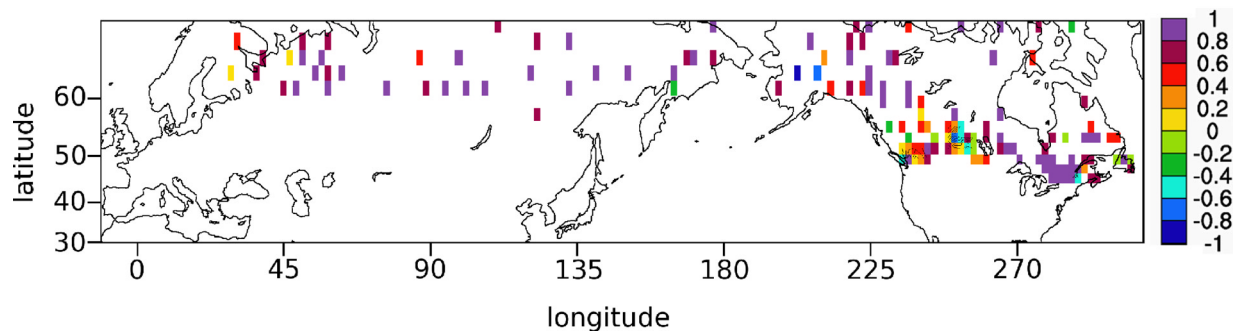
Figure 7. Local linear correlation between the in situ snow depth and the emissivity difference at horizontal polarization (19H−37H) for all available stations during the 1992–1993 winter season.
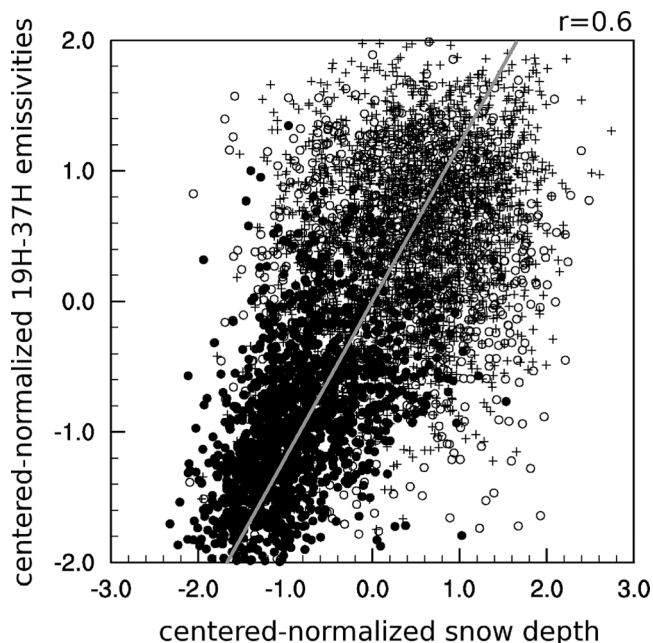
Figure 8. Global linear correlation between the normalized in situ snow depth and the normalized emissivity difference at horizontal polarization (19H−37H) for the 1992–1993 winter season. The correlation coefficient is indicated.

components need to be used, representing a total of 99.5% of the variance. Once the components are extracted by the PCA, each monthly snow depth map can be represented by the weighted sum of the first 50 PCA components. For each month and for the year 1992–1993, a minimization procedure based on a quasi-Newton method is then used to minimize the difference between the in situ measurements and the ISBA derived snow depth PCA-representation. The minimization has been performed for the three previous cases (globally, Eurasia, and North America). The correlation between the resulting snow depth and the in situ snow depth measurements is very satisfactory for Eurasia (∼0.8),

less over North America (<0.6) and globally. Table 2 shows the improvement of the statistics with optimized ISBA. The correlations are usually better while the biases are closer to zero as compared to the genuine ISBA: the Root Mean Square (RMS) errors are thus lower in the optimized version. Mitigated results for America are due to a lower density of stations and a more complex snow cover variability (coastal influence due to smaller coast-to-coast distance in North America, less strong topographic gradient in Eurasia). In the following, we focus on the Eurasian case since a more detailed spatial study would be required for the global or the American cases.

[29] Calibrating the ISBA outputs is not the main goal here: we optimize ISBA outputs for interpolating the local statistics outside the in situ stations. However, it should be noticed that, by design, the optimized ISBA outputs are much closer to in situ measurements (Table 2): this calibration technique is interesting by itself for any model calibration to sparse in situ measurements. Over Eurasia and for each pixel, the mean and standard deviation of the snow depth are derived from our optimized ISBA-ES estimates. The improvement of the local statistics is represented in Table 3. The RMS errors decrease, from the original ISBA-ES prediction to the optimized configuration, from 5.9 (respectively 6.0) to 3.6 (resp. 4.2) for the mean (resp. standard deviation). The quality of these local statistics is now more compatible with inversion experiments.

[30] We tested different inversion methods to derive the snow depth from satellite observations: linear, multilinear, and various neural networks. Neural Networks (NN) give the best results since they offer a better ability to merge the information. The chosen NN has 7 inputs (i.e., satellite observations), 30 units in the hidden layer, and 1 output (i.e., the standardized snow depth estimate). The inputs are the standardized emissivities at 19H, 37H, 85H, 19H−37H and 37H−85H derived from SSM/I, the backscattering coefficient (ERS) and the visible reflectances (AVHRR). For each pixel, both the inputs and output are standardized (i.e., centered and normalized) by their respective (interpolated) local statistics. The learning phase of the NN uses 75% of the database composed of the satellite observations

Table 2. Summary of the Statistics of the Prediction Methods for the 25% of the Data With Which These Methods Have Been Evaluated for the Winter 1992–1993[a]

| | In Situ | | ISBA Retrievals | | | | | | | | Satellite Retrievals: NN | | | |
| | | | ISBA | | | | ISBA − 50 PC opt | | | | | | | |
Month 1992/1993	μ_{SD}	σ_{SD}	ρ	b	σ	RMS	ρ	b	σ	RMS	ρ	b	σ	RMS
Jul	0.0	0.0	ND	0.0	0.0	0.0	ND	0.0	0.1	0.1	0.06	1.6	3.3	3.7
Aug	0.0	0.0	ND	0.0	0.0	0.0	ND	0.0	0.1	0.1	0.12	1.9	4.4	4.8
Sep	0.0	0.2	0.76	0.0	0.2	0.2	0.59	0.0	0.2	0.2	0.22	2.1	4.2	4.7
Oct	1.9	3.9	0.87	0.0	2.5	2.5	0.89	0.0	1.8	1.8	0.78	1.8	5.1	5.4
Nov	9.1	11.7	0.91	1.2	5.6	5.7	0.97	0.0	3.0	3.0	0.88	0.8	6.2	6.2
Dec	15.8	16.1	0.88	2.9	8.6	9.1	0.95	−0.4	5.1	5.1	0.86	0.0	3.9	3.9
Jan	22.8	21.0	0.86	3.6	11.1	11.7	0.93	0.0	7.8	7.8	0.90	1.3	7.9	8.0
Feb	28.6	26.7	0.85	2.5	14.5	14.7	0.92	0.0	10.6	10.6	0.93	−1.3	9.7	9.8
Mar	26.4	27.7	0.73	−3.2	18.7	19.0	0.91	0.8	11.4	11.4	0.94	−0.5	9.7	9.8
Apr	13.6	23.7	0.59	−4.9	19.8	20.4	0.89	1.0	10.8	10.8	0.91	0.8	9.7	9.7
May	1.9	8.7	0.68	−0.7	6.4	6.4	0.97	0.0	2.3	2.3	0.90	2.3	5.8	6.2
Jun	0.0	0.0	ND	0.0	0.0	0.0	ND	0.0	0.4	0.4	0.00	1.7	3.8	4.1

[a]ρ, the linear correlation; b, the bias; σ, the standard deviation; RMS, the root mean square error; In Situ, the mean and the standard deviation of the in situ measurements for all the stations; ISBA column, genuine predictions of the model; ISBA − 50 CP opt, the ISBA configuration with 50 optimized components; NN column, the neural network prediction with 7 inputs.

Table 3. Summary of the Statistics of the Estimates of the Local Statistics (Local Mean μ and Standard Deviation σ) for the Three Configurations of ISBA-ES Predictions[a]

| | Eurasia | | | | | |
| | μ | | | σ | | |
Configuration	ρ	b	RMS	ρ	b	RMS
ISBA genuine	0.84	0.2	5.9	0.85	0.8	6.0
ISBA 50 PC	0.84	0.2	6.0	0.85	0.8	5.9
ISBA 50 PC + optimization	0.94	0.2	3.6	0.93	−0.1	4.2

[a]ρ, the linear correlation; b, the bias; RMS, the root mean square error; ISBA genuine, genuine predictions of the model; ISBA 50 PC, the ISBA predictions projected in the first 50 Principal Components; ISBA 50 PC + optimized, the ISBA projection with 50 optimized components.

and the in situ snow depth in coincidence. The generalization database uses the last 25% to test the ability of the NN retrieval scheme to generalize its behavior to unknown data.

[31] The statistics of the inversion are indicated in Table 2. Similar results are found between the snow depth prediction of optimized ISBA-ES and those derived from satellite observations, especially for the winter months with significant snow. For the months with a low level of snow, optimized ISBA shows a really good agreement as opposed to satellite-derived NN inversion which focuses on higher contents by design. During the winter, the bias is usually negligible with optimized ISBA and gets close to 2 cm for many months with NN. The lower performance of the approaches at the end of the season is related to the fact that the 37 GHz signal starts to be sensitive to the scattering by large particles at this period of the winter, and thus does not react anymore to the snow depth. These differences between the NN and the optimized-ISBA approaches are due mainly to the annual learning of NN in opposition to the monthly optimization of ISBA which is a huge advantage. However, RMS is always less than 10.0 cm for the NN inversions while optimized ISBA reaches 11.4 cm in March. The methodology is actually only limited by the number and quality of in situ measurements. (If the database of measurements was larger, the NN learning could, for example, be done on a monthly scale rather than on the whole year. This would have a strong impact on the results.) More important, optimization of ISBA monthly outputs will always require calibration by in situ measurements whereas our retrieval is ready to use for other periods of time, without any additional in situ information.

[32] Figures 9a and 9b compare SD time series during the winter, from in situ measurements and from the NN retrievals. Figure 9a presents retrievals with limited success, illustrating the limitations of the technique. For instance, in one case (black circles), in situ SD has a smooth standard behavior whereas the inverted SD presents abrupt variations. For two of these cases (circles and triangles), the snow accumulation is rather important: high snow depths are often incorrectly predicted since they are rare in the learning database and as a consequence the NN has not a good statistical representation of them. On the third example (white circles), the snow melting is predicted too early. Figure 9b shows examples of successful inversions that represent the majority of cases. For these cases, the time series of retrieved SD are coherent with the in situ measurements. One case (black circles) illustrates the capacity of the

algorithm to estimate the absence of snow. Another (triangles) demonstrates the expected performance of the NN for commonly observed seasonal cycles of SD. The third example (white circles) shows that the algorithm can also correctly detect two maxima in the seasonal cycle.

[33] Figure 10 presents the predicted snow depths for December 1992 over Eurasia, as compared to in situ measurements. The patterns observed in the in situ data, are also present on the neural network retrieved products. For example, the area with significant snow depths near 90°E and 65°N is correctly reproduced. The snow depth gradient south of 60°N agrees also very well with the in situ observations. However over some regions, the retrieval does not perform well: for instance over Kamchatka (160°E, 55°N), the measured snow depths are less than 30 cm whereas the satellite inversion predicts values close to 50 cm.

[34] Finally, an important point to be made is that globally the satellite retrieval is better than the ISBA prediction alone. This means that satellite observations provide additional information on the snow depth and that this information could benefit land surface model outputs. Variational assimilation of satellite observations in surface models would improve the quality of the simulations, by taking profit of both model and satellite observation potentials. This could be done either by direct assimilation of the satellite observations (although that can be hampered by the lack of accurate radiative transfer models for the snow) or by assimilation of the retrieved snow depth products provided that related uncertainties are estimated [*Aires et al.*, 2004].

5. Satellite-Derived Snow Classification

[35] Snow classifications using passive microwave observations have already been developed based directly on SSM/I brightness temperatures up to 37 GHz, using linear [i.e., *Neale et al.*, 1990] or more sophisticated classification method [*Sun et al.*, 1997]. Classification results do not directly translate into quantifiable properties but they can yield valuable qualitative information on the snow properties. Additional information that is not directly measured remotely can be deduced from them. It is a synthetic method to compress the information: each cluster of snow will summarize a specific set of snow characteristics. It can give indications to modelers (climate and hydrology), each cluster of snow being related to specific snow properties that can help parameterization in the model.

[36] In addition, snow cover classification can be a first step toward the development of snow retrieval algorithms. The classification then helps group pixels with similar satellite signatures (i.e., with limited variability) and a specific algorithm is developed for each class. This has also been suggested by *Kelly et al.* [2003].

[37] We apply an unsupervised (i.e., without a priori on the classes) clustering technique to the microwave satellite observations on a monthly basis: the emissivities at 19, 37, 85 GHz at horizontal polarizations, the emissivity differences (19H−37H and 37H−85H), and the microwave backscattering coefficient are used for the clustering. Only pixels that are completely covered by snow during the month are considered. *Kohonen* [1984] topological method,
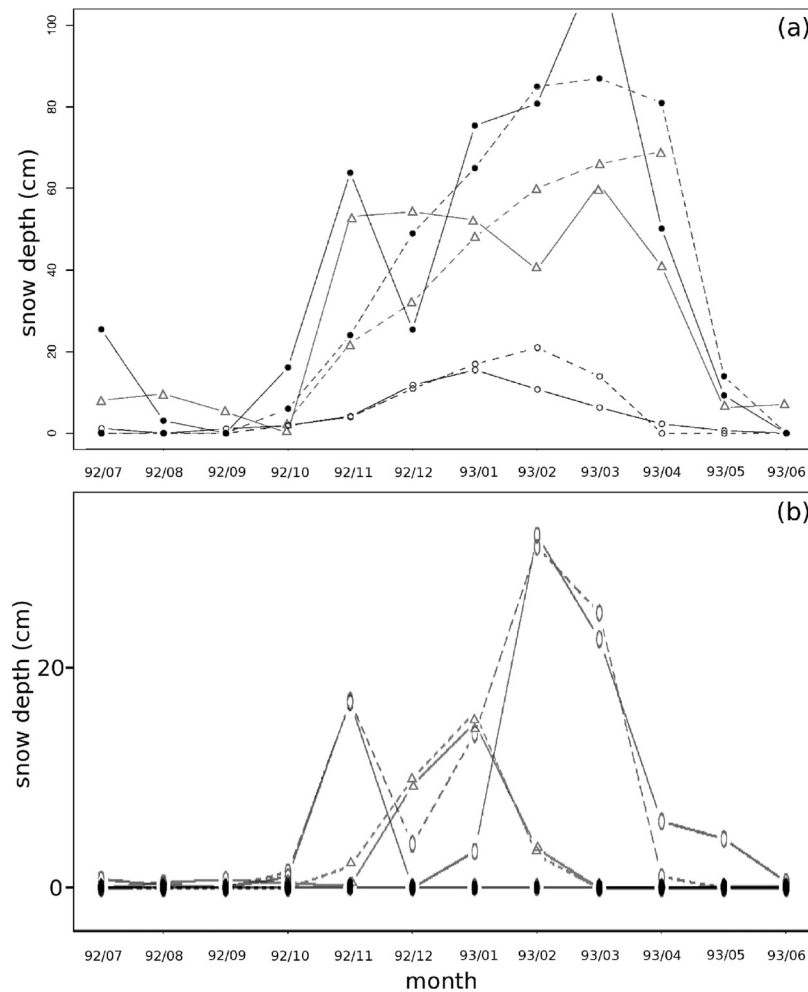
Figure 9. Samples of in situ (dashed lines) and retrieved (solid lines) snow depth time series for the 1992–1993 winter. (a) Not correctly predicted. (b) Correctly predicted.

also called self-organizing maps have already been used to analyze satellite data sets [*Prigent et al.*, 2001]. The special feature of this classification algorithm is that neighborhood requirement is imposed on the clusters, so that when it converges, prototypes corresponding to nearby classes have nearby location in the data space: this additional information helps interpret the classes. Using this Kohonen classification, for each month and each location, a snow cluster is associated to the satellite observations. The clustering technique synthesizes all the observations to obtain an analysis of the variations of one spectral band with respect to the others and gives insight into the relationships between the observations. The number of classes is chosen so that for each cluster, at least one information provides statistical discrimination, thus limiting ambiguities between clusters. Figure 11 shows the variation of the center of each cluster for each piece of information along with its standard deviation around the center value. The visible information has not been used for the clustering because it is not always present over northern latitudes. However, for each class, the variation of the visible reflectances, when present, is indicated in Figure 11d. The standard deviation of the visible

reflectances in each cluster is large, as expected, because this channel is not used in the classification.

[38] For 3 different months in the winter, for each snow-covered pixel, Figures 12b–12d shows the result of the clustering. Figure 12a indicates for each location the snow cluster that is more frequent during the winter. The snow classification by *Sturm et al.* [1995] and the vegetation classification by *Matthews* [1983] are added to Figures 12e and 12f.

[39] From cluster 1 to cluster 8, there is a clear increase of the scattering contribution, especially at 37 and 85 GHz, likely related to increasing grain sizes in the snowpack: in Figure 11a the 37 and 85 GHz emissivities decreases from cluster 1 to cluster 8. For the last classes (6 to 8), the 85 GHz emissivity reaches saturation while the 37 GHz emissivity still decreases. This is also observed on the 37H–85H emissivity difference (Figure 11b) that first increases (because of stronger scattering at 85 GHz) and then decreases (with the 85 GHz emissivity saturating with the 37 GHz emissivity still decreasing). The backscattering coefficient decreases from cluster 1 to 8 because of the topographic influence. Anticorrelation between the visible reflectances and the 85 GHz emissivities is clear (see Figures 11a and
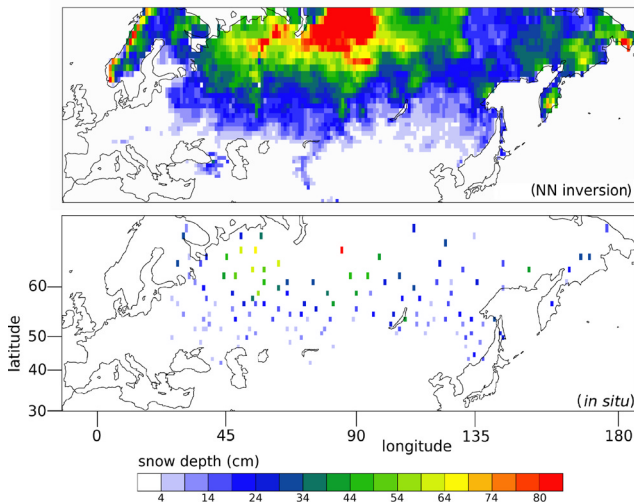
Figure 10. Map of the snow depths retrieved from the satellite observations using a Neural Network method along with the in situ measurements for December 1992 over Eurasia, as compared to the in situ measurements.

11d). The following analysis tends to show that these successive clusters are related to the snow aging.

[40] From the beginning of the winter to its end, there is a clear trend toward larger proportion of high snow classes in Figure 12: at the beginning of the winter, classes 1 to 5 dominate but are then progressively replaced by higher classes.

[41] Cluster 1 is characterized by high emissivities close to vegetation emissivities (Figure 11). It is predominantly located in regions dominated by forests, both evergreen and deciduous (in the *Matthews* vegetation classification, see Figure 12), in the beginning of the winter. A few areas (north and north east of the Great Lake for instance or the Ural Mountains) that are covered by evergreen forest belong to cluster 1 all winter long. Snow cluster 2 is similar to cluster 1 and is almost always located in the regions surrounding the cluster 1 regions: it is a transition cluster between classes 1 and 3, located in regions of less dense vegetation, in the transition zone between forest and woodland/tundra. Class 3 corresponds to dryer snow: it is present at rather high latitude at the beginning of the winter and in the middle of the winter at lower latitude (Figure 12). It is characterized by significant scattering at 37 and 85 GHz (i.e., dry snow with rather large grains) and higher visible reflectivities. The Yenisey River Valley in Russia (around 90°E) belongs to that cluster all winter long. Cluster 5 covers the northern latitude at the beginning of the snow season and is dominant southward in the middle of the winter: it has almost disappeared at the end of the winter. On the contrary, clusters 7 and 8 are rarely present in the

Figure 11. Result of the multisatellite classification. (a–c) Variation of the center of each cluster for each piece of information along with its standard deviation around the center value. (d) Corresponding values for the visible reflectances.
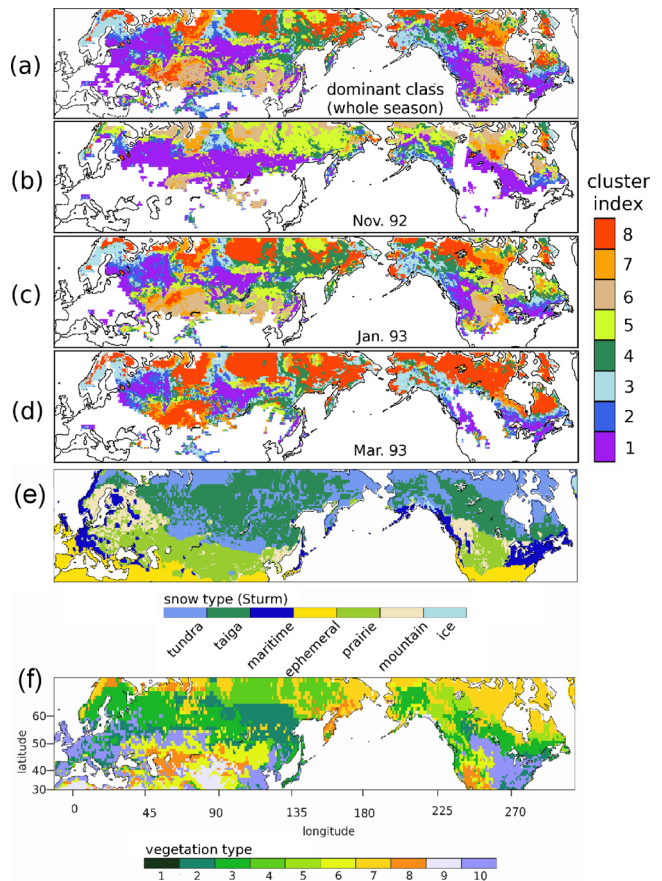
Figure 12. Maps of the clustering results. (a) Dominant class for the winter, (b–d) the results for 3 different months in the winter, (e) the snow classification by *Sturm et al.* [1995], and (f) the vegetation classification by *Matthews* [1983].
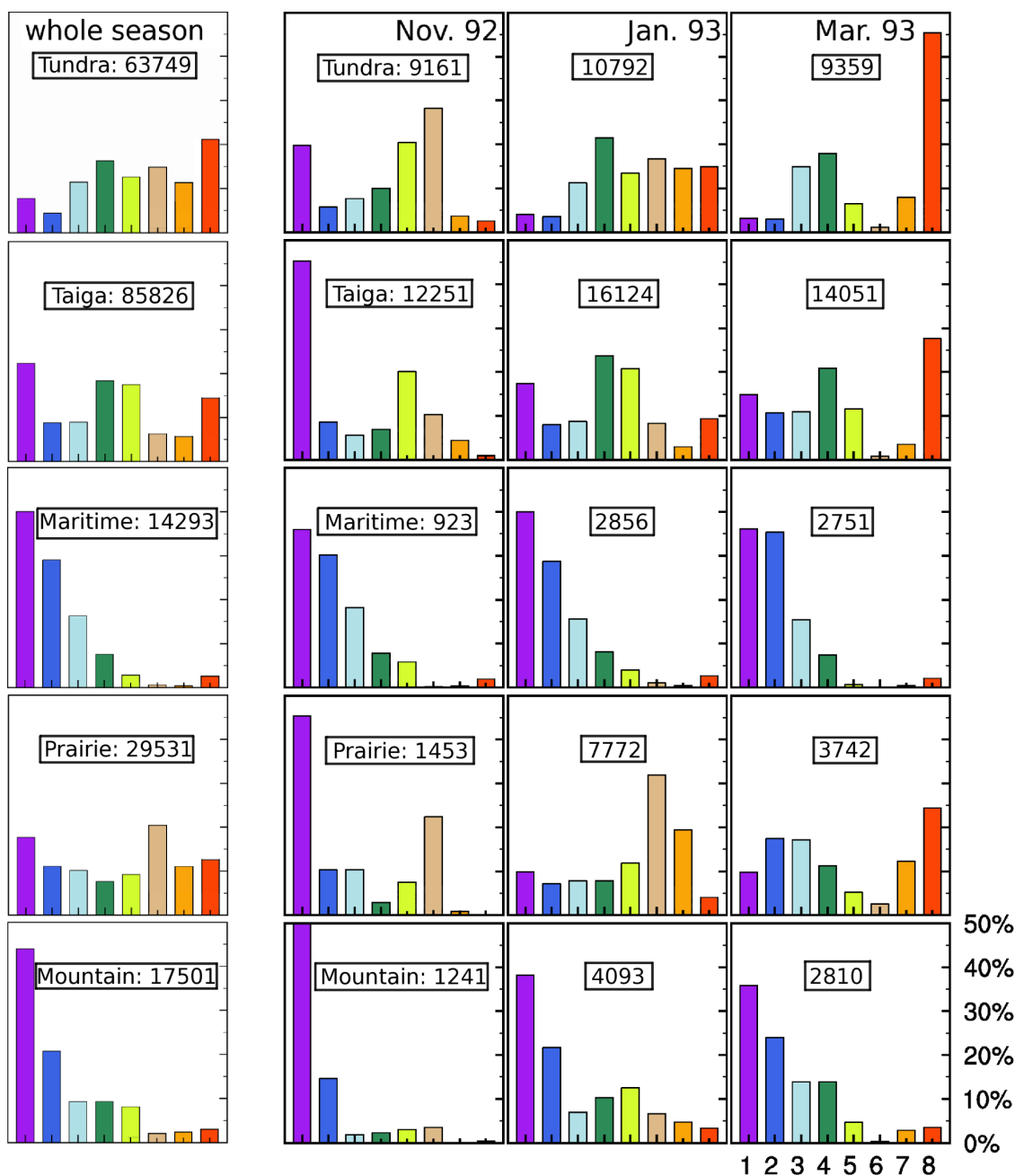
Figure 13. Distribution of the classes deduced from the microwave satellite observations for each dominant class in the *Sturm et al.* [1995] classification. From left to right are distributions for the whole winter season, for November, for January, and for March.

beginning of the snow season: for these clusters, emissivities at 37 and 85 GHz are of the same order (lower emissivity differences between 37 and 85 GHz) and the 19 GHz emissivity also decreases indicating the presence of large grains.

[42] How does this satellite-derived classification compare with the static snow classification from *Sturm et al.* [1995]? For the most representative classes in the Sturm et al. classification, Figure 13 gives the percentage of each satellite-derived clusters for 3 months in the winter, along with the cumulative percentage for the whole winter (left column). As already described, for the tundra, taiga, and

prairie classes in the Sturm et al. classification, the proportion of high classes in the satellite-derived classification increases as the snow ages. This clearly shows that for a given cluster in the Sturm et al. classification, the snow parameters that influence the microwave emissivities evolve significantly: depending on the snow classification application, using a satellite-derived classification that describes the snow evolution during the winter might be more adequate. The maritime snow type however is particularly stable all winter long, the mountain type as well but to a lower extent. This snow type could be interpreted as the mountain snow type with a strong influence of the cluster 8,

associated to metamorphism. This stability through the season is due to the proximity of the coast which generates a high precipitation rate and air temperatures close to zero. One will also notice abrupt transitions in the satellite-derived classification that do not appear on the Sturm et al. one. For example, during most of the winter, the satellite signatures are significantly different east and west of Lena River (around 120°E in Russia): this transition, although not present on the Sturm et al. classification certainly corresponds to real changes in the snow properties.

[43] The satellite-derived snow classification summarizes the spatial and temporal variability of the snowpack during the winter season. It is a synthetic method to derive snow information that is not directly measurable, that is not captured by static snow classification although this information can be very relevant for modeling activities. For instance, *Sud and Mocko* [1999] attribute the delay in snow melt in the models partly to neglecting the snow aging on the thermal diffusivity and albedo: using the satellite-derived snow classification would make it possible for each snow covered location to give an indication on the snow aging.

6. Conclusions and Perspectives

[44] The sensitivity of passive microwave satellite observations to snow characteristics has been systematically analyzed, for a whole snow season in the Northern Hemisphere. The emissivities have been first calculated from the measured brightness temperatures from SSM/I, thus suppressing the variable contribution of the atmosphere and surface temperature from the signal. The analysis includes the 85 GHz measurements, that is often neglected because of its higher sensitivity to the atmosphere. Coincident satellite-derived visible reflectances and active microwave backscattering coefficients are also examined to help understand the passive microwave signatures.

[45] The emissivity at 85 GHz strongly reacts to the presence of snow as soon as it covers the ground.

[46] Vegetation does interfere with the signal that is received by the satellite. Snow emissivities also react to scattering by the snow grain growth related to the snow metamorphism during the winter. This phenomenon increases with frequency and is already very sensitive at 37 GHz.

[47] Comparison with in situ snow depth measurements shows low correlation with the microwave emissivities on a global basis. As a consequence, snow depth retrieval is very difficult to retrieve with accuracy from passive microwave observations only, on a global basis for the full snow season, confirming previous studies [e.g., *Kelly et al.*, 2003; *Grippa et al.*, 2004]. To partly alleviate these difficulties, a scheme is developed that combines satellite observations, in situ measurements, and land surface models. This retrieval method is very general and can be used for any other applications for which there is a need to merge the satellite observations with sparse in situ measurements and model outputs. Furthermore, the combination of different wavelengths partly limits the ambiguities related to the individual sensitivity of each satellite observation to the various sources of variability (snow depth, vegetation, snow metamorphism, among others). The final retrieval algorithm

is compatible with an assimilation strategy that can better constrain the behavior of surface models.

[48] The microwave observations can also help characterize the snow physical properties. A clustering algorithm is applied to the microwave satellite observations for a whole snow season for the Northern Hemisphere and clearly shows a strong sensitivity to the snow metamorphism during the winter. Given that the snow metamorphism drives the snow cover evolution, first its albedo and second its mechanical properties, characterization of the snowpack using satellite observation classification can yield qualitative information for snow model parameterization.

References

Aires, F., C. Prigent, and W. B. Rossow (2004), Neural network uncertainty assessment using Bayesian statistics with application to remote sensing: 2. Output errors, *J. Geophys. Res.*, *109*, D10304, doi:10.1029/2003JD004174.

Aires, F., C. Prigent, and W. B. Rossow (2005), Sensitivity of satellite microwave and infrared observations to soil moisture at a global scale: 2. Global statistical relationships, *J. Geophys. Res.*, *110*, D11103, doi:10.1029/2004JD005094.

Aoki, T., M. Fukabori, A. Hachikubo, Y. Tachibana, and F. Nishio (2000), Effects of snow physical parameters on spectral albedo and bidirectional reflectance of snow surface, *J. Geophys. Res.*, *105*, 10,219–10,236.

Armstrong, R. (2001), Historical Soviet Daily Snow Depth Version 2 (HSDSD) [CD-ROM], Natl. Snow and Ice Data Cent., Boulder, Colo.

Boone, A., and P. Etchevers (2001), An intercomparison of three snow schemes of varying complexity coupled to the same land-surface model: Local scale evaluation at an Alpine site, *J. Hydrometeorol.*, *2*, 374–394.

Brown, R. (2000), Canadian Snow Data [CD-ROM], CRYSYS Proj., Clim. Processes and Earth Obs. Div., Meteorol. Serv. of Canada, Downsview, Ont., Canada.

Brubaker, K. L., M. Jasinski, A. T. C. Chang, and E. Josberger (2000), Interpolating sparse surface measurements for calibration and validation of satellite-derived snow water equivalent in Russian Siberia, paper presented at Remote Sensing in Hydrology Symposium, Int. Assoc. of Hydrol. Sci., Santa Fe, N. M.

Chang, A. T. C., P. Gloersen, T. Schmugge, T. T. Wilheit, and H. J. Zwally (1976), Microwave emission from snow and glacier, *J. Glaciol.*, *16*, 23–39.

Chang, A. T. C., J. L. Foster, and D. K. Hall (1987), Nimbus-7 SSMR derived global snow cover parameters, *Ann. Glaciol.*, *9*, 39–44.

Cline, D. W., and T. R. Carroll (1999), Inference of snow cover beneath obscuring clouds using optical remote sensing and a distributed snow energy and mass balance model, *J. Geophys. Res.*, *104*, 19,631–19,644.

Douville, H., J.-F. Royer, and J.-F. Mahfouf (1995), A new snow parameterization for the Météo-France climate model, *Clim. Dyn.*, *12*, 21–35.

Foster, J., G. Liston, R. Koster, R. Essery, H. Behr, L. Dumenil, D. Verseghy, S. Thompson, D. Pollard, and J. Cohen (1996a), Snow cover and snow mass intercomparisons of general circulation models and remotely sensed datasets, *J. Clim.*, *9*, 409–426.

Foster, J., R. Koster, H. Behr, L. Dumenil, J. Cohen, R. Essery, G. Liston, S. Thompson, D. Pollard, and D. Verseghy (1996b), Snow-mass intercomparisons in the boreal forests from general circulation models and remotely sensed data sets, *Polar Record*, *32*, 199–208.

Frei, A., and D. A. Robinson (1999), Northern Hemisphere snow extent: Regional variability, *Int. J. Climatol.*, *34*, 1535–1560.

Gong, G., D. Entekhabi, J. Cohen, and D. Robinson (2004), Sensitivity of atmospheric response to modeled snow anomaly characteristics, *J. Geophys. Res.*, *109*, D06107, doi:10.1029/2003JD004160.

Grippa, E., N. Mognard, T. Le Thoan, and E. Josberger (2004), Siberia snow depth climatology derived from SSM/I data using a combined dynamic and static algorithm, *Remote Sens. Environ.*, *93*, 30–41.

Grody, N. C., and A. N. Basist (1996), Global identification of snowcover using SSM/I measurements, *IEEE Trans. Geosci. Remote Sens.*, *34*, 237–249.

Hall, D. K., M. Sturm, C. S. Benson, A. T. C. Chang, J. L. Foster, H. Garbeil, and E. Chacho (1991), Passive microwave remote and in situ measurements of Arctic and Subarctic snow covers in Alaska, *Remote Sens. Environ.*, *38*, 161–172.

Hewison, T. J., and S. J. English (1999), Airborne retrievals of snow and ice surface emissivity at millimeter wavelengths, *IEEE Trans. Geosci. Remote Sens.*, *37*, 1871–1887.

Hollinger, J. P., R. Lo, G. Poe, R. Savage, and J. Pierce (1987), Special Sensor Microwave/Imager user's guide, Nav. Res. Lab., Washington, D. C.

James, M. E., and S. N. V. Kalluri (1994), The Pathfinder AVHRR land data set: An improved coarse resolution data set for terrestrial monitoring, *Int. J. Remote Sens.*, *15*, 3347–3364.

Josberger, E. G., and N. M. Mognard (2002), A passive microwave snow depth algorithm with a proxy for snow metamorphism, *Hydrol. Processes*, *16*, 1557–1568.

Judge, J., J. F. Galantowicz, A. W. England, and P. Dahl (1997), Freeze/ thaw classification for prairie soils using SSM/I radiobrightness, *IEEE Trans. Geosci. Remote Sens.*, *35*, 827–832.

Kalnay, E., et al. (1996), The NCEP/NCAR 40-year reanalysis project, *Bull. Am. Meteorol. Soc.*, *77*, 437–470.

Kelly, R. E. J., and A. T. C. Chang (2003), Development of a passive microwave global snow depth retrieval algorithm for Special Sensor Microwave Imager (SSM/I) and Advanced Microwave Scanning Radiometer-EOS (AMSR-E) data, *Radio Sci.*, *38*(4), 8076, doi:10.1029/ 2002RS002648.

Kelly, R. E., A. T. C. Chang, L. Tsang, and J. Foster (2003), A prototype AMSR-E global snow area and snow depth algorithm, *IEEE Trans. Geosci. Remote Sens.*, *41*, 230–242.

Kohonen, T. (1984), *Self-Organization and Associative Memory*, Springer, New York.

Kunzi, K. F., S. Patil, and H. Rott (1982), Snow-cover parameter retrieved from Nimbus-7 Scanning Multichannel Microwave Radiometer (SMMR) data, *IEEE Trans. Geosci. Remote Sens.*, *4*, 452–467.

Kurvonen, L., and M. Hallikainen (1997), Influence of land-cover category of brightness temperature of snow, *IEEE Trans. Geosci. Remote Sens.*, *35*, 367–377.

Matthews, E. (1983), Global vegetation and land use: New high-resolution data bases for climate studies, *J. Clim. Appl. Meteorol.*, *22*, 474–486.

Matzler, C. (1994), Passive microwave signatures of landscapes in winter, *Meteorol. Atmos. Phys.*, *54*, 241–260.

Neale, C. M. U., M. J. McFarland, and K. Chang (1990), Land surface type classification using microwave brightness temperatures from the Special Sensor Microwave/Imager, *IEEE Trans. Geosci. Remote Sens.*, *28*, 829–838.

Prigent, C., W. B. Rossow, and E. Matthews (1997), Microwave land surface emissivities estimated from SSM/I observations, *J. Geophys. Res.*, *102*, 21,867–21,890.

Prigent, C., F. Aires, W. B. Rossow, and E. Matthews (2001), Joint characterization of vegetation by satellite observations from visible to microwave wavelength: A sensitivity analysis, *J. Geophys. Res.*, *106*, 20,665–20,685.

Pulliainen, J., and M. Hallikainen (2001), Retrieval of regional snow water equivalent from space-borne passive microwave observations, *Remote Sens. Environ.*, *75*, 76–85.

Robinson, D. A., and T. E. Spies (1994), Monitoring snow cover on the Tibetan Plateau using passive microwave satellite data, paper presented at ESA/NASA International Workshop, Zeist, Netherlands.

Robinson, D. A., F. T. Keiming, and R. R. Heim (1993), Global snow cover monitoring: An update, *Bull. Am. Meteorol. Soc.*, *74*, 1689–1696.

Rosenfeld, S., and N. Grody (2000), Anomalous spectra of snow cover observed from Special Sensor Microwave/Imager measurements, *J. Geophys. Res.*, *105*, 14,913–14,925.

Rossow, W. B., and R. A. Schiffer (1999), Advances in understanding clouds from ISCCP, *Bull. Am. Meteorol. Soc.*, *80*, 2261–2287.

Schanda, E., C. Matzler, and K. Kunzi (1983), Microwave remote sensing of snow cover, *Int. J. Remote Sens.*, *4*, 149–158.

Schmidlin, T. (1990), A critique of the climatic record of water equivalent of snow on the ground in the United States, *J. Appl. Meteorol.*, *29*, 1136–1141.

Singh, P. R., and T. Y. Gan (2000), Retrieval of snow water equivalent using passive microwave brightness temperature data, *Remote Sens. Environ.*, *74*, 275–286.

Sturm, M., and C. S. Benson (1997), Vapor transport, grain growth and depth-hoar development in the subarctic snow, *J. Glaciol.*, *43*, 42–48.

Sturm, M., J. Holmgren, and G. E. Liston (1995), A seasonal snow cover classification system for local to global application, *J. Clim.*, *8*, 1261–1283.

Sud, Y. C., and D. M. Mocko (1999), New snow-physics to complement SiB. Part I: Design and evaluation with ISLSCP Initiative I dataset, *J. Meteorol. Soc. Jpn.*, *77*, 335–348.

Sun, C., C. M. U. Neala, J. McDonnell, and H.-D. Cheng (1997), Monitoring land-surface snow conditions from SSM/I data using an artificial neural network classifier, *IEEE Trans. Geosci. Remote Sens.*, *35*, 801–809.

Tsang, L. (1992), Dense media radiative transfer theory for dense discrete random media with spherical particles of multiple sizes and permittivities, in *Progress in Electromagnetics Research*, vol. 6, pp. 181–230, Elsevier, New York.

_____

F. Aires, CNRS/IPSL/Laboratoire de Météorologie Dynamique, Université Paris VI, 4, place Jussieu, F-75252 Paris Cedex 05, France. (filipe.aires@lmd.jussieu.fr)

E. Cordisco and C. Prigent, Centre National de la Recherche Scientifique, Laboratoire d'Études du Rayonnement et de la Matière en Astrophysique, Observatoire de Paris, 61, avenue de l'Observatoire, F-75014 Paris, France. (emmanuel.cordisco@obspm.fr; catherine.prigent@obspm.fr)